Supplementary Information (SI) for Journal of Materials Chemistry A.
This journal is © The Royal Society of Chemistry 2025

Supplementary Information

Ultra-Stable Solid-State Lithium Metal Batteries with Ferroelectric Oxide-Enhanced PVDF-Based Hybrid Solid Electrolytes

Jie Zhao [a], Saifang Huang[a], Yuyan Zhao [b], Can Cui [a, c]*, Yudong Zhang [a], Haiqin Lin [a], Cuijiao Zhao [a], Weiji Dai [a], Zhuofeng Liu [e], Xin Song [d], and Peng Cao [d,f]**

[a] School of Materials Science and Engineering, Jiangsu University of Science and Technology, Zhenjiang 212100, China

[b] Suzhou Institute for Advanced Research, University of Science and Technology of China, Suzhou 215123, China

[c] Key Laboratory of Advanced Energy Materials Chemistry (Ministry of Education), Nankai University, Tianjin 300071, China

[d] Department of Chemical & Materials Engineering, The University of Auckland, Private Bag 92019, Auckland 1142, New Zealand

[e] College of Aerospace Science and Engineering, National University of Defense Technology, Changsha 410073, China

[f] MacDiarmid Institute of Advanced Materials and Nanotechnology, Victoria University Wellington, PO Box 600, Wellington 6140, New Zealand

* Corresponding authors. E-mail: s.huang@just.edu.cn (S. Huang), cuican@just.edu.cn (C. Cui), p.cao@auckland.ac.nz (P. Cao)

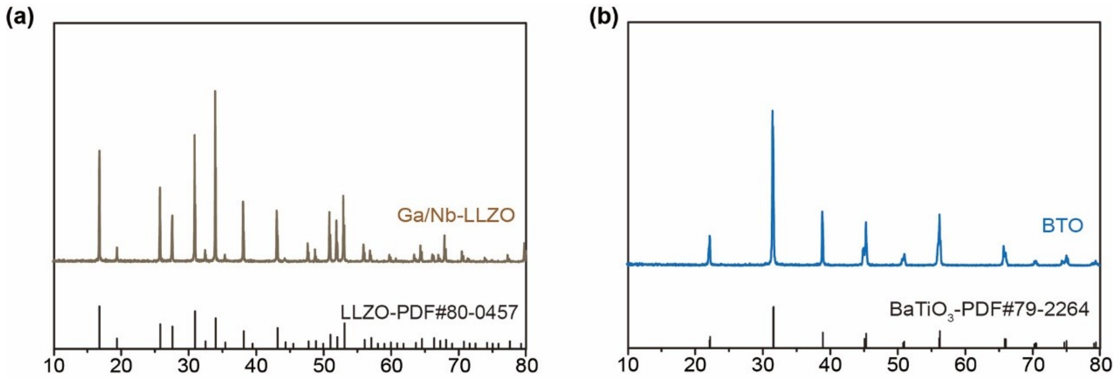

Fig. S1 X-ray diffraction (XRD) analysis of (a) Ga/Nb-LLZO and (b) BTO inorganic nanoparticle.

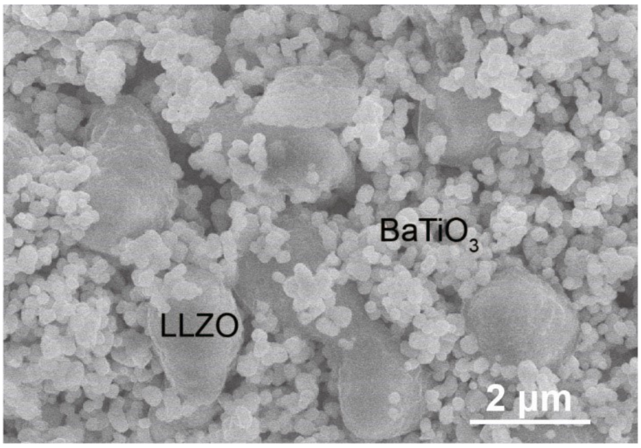

Fig. S2 SEM images of pre-mixed Ga/Nb-LLZO and BTO inorganic nanoparticle

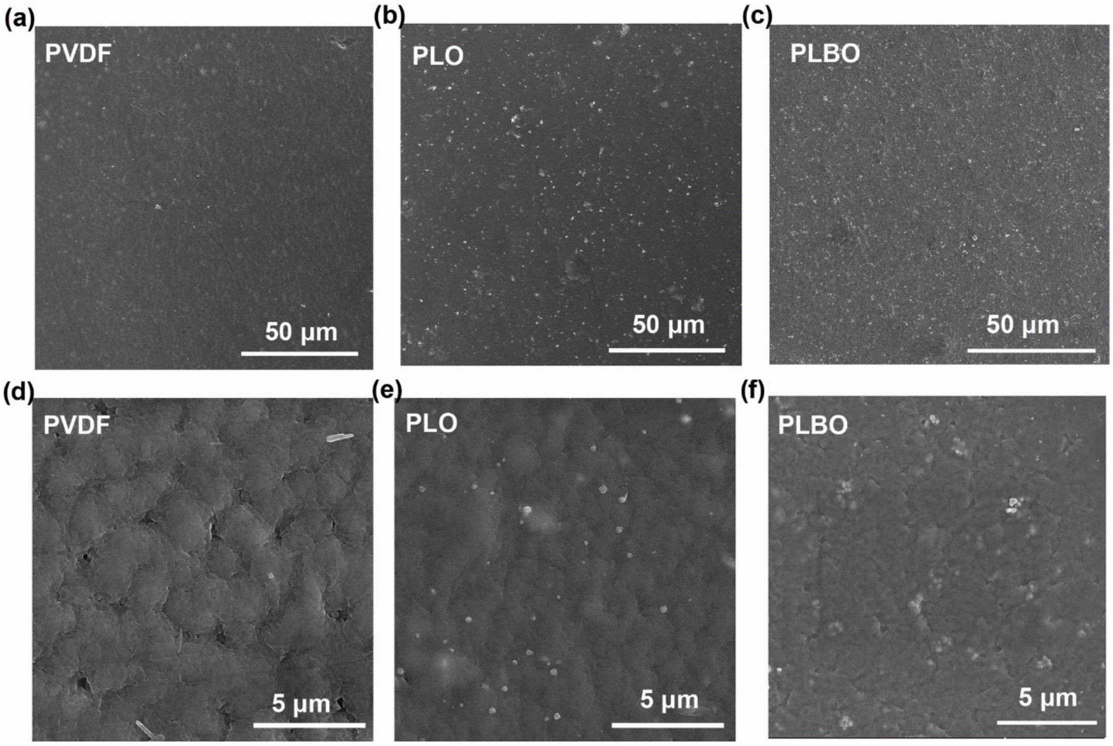

Fig. S3 Top-view SEM images of the (a, d) PVDF, (b, e) PLO and (c, f) PLBO membranes.

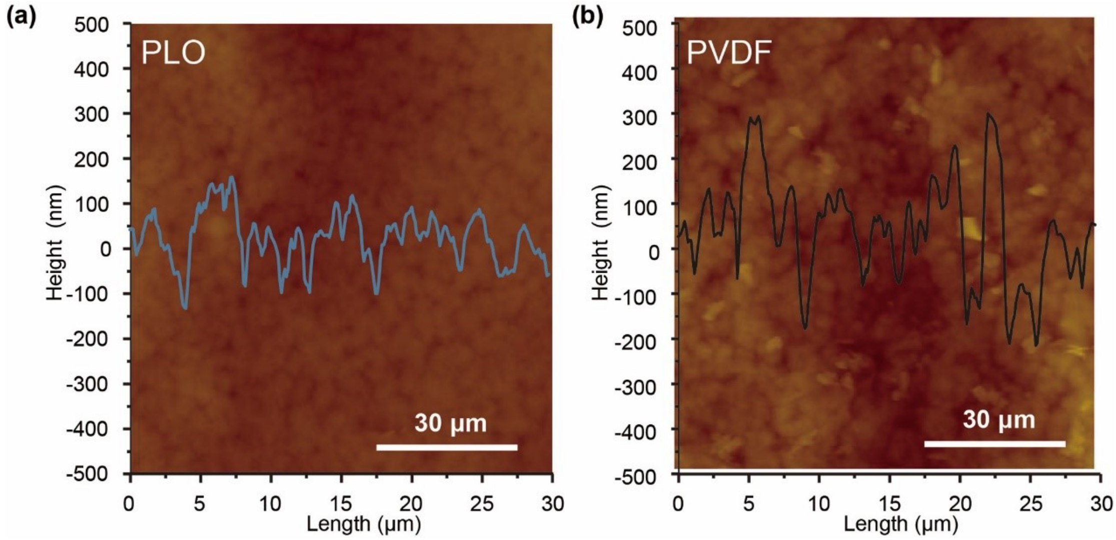

Fig. S4 AFM image and height profile (inset) of the (a) PLO and (b) PVDF membranes.

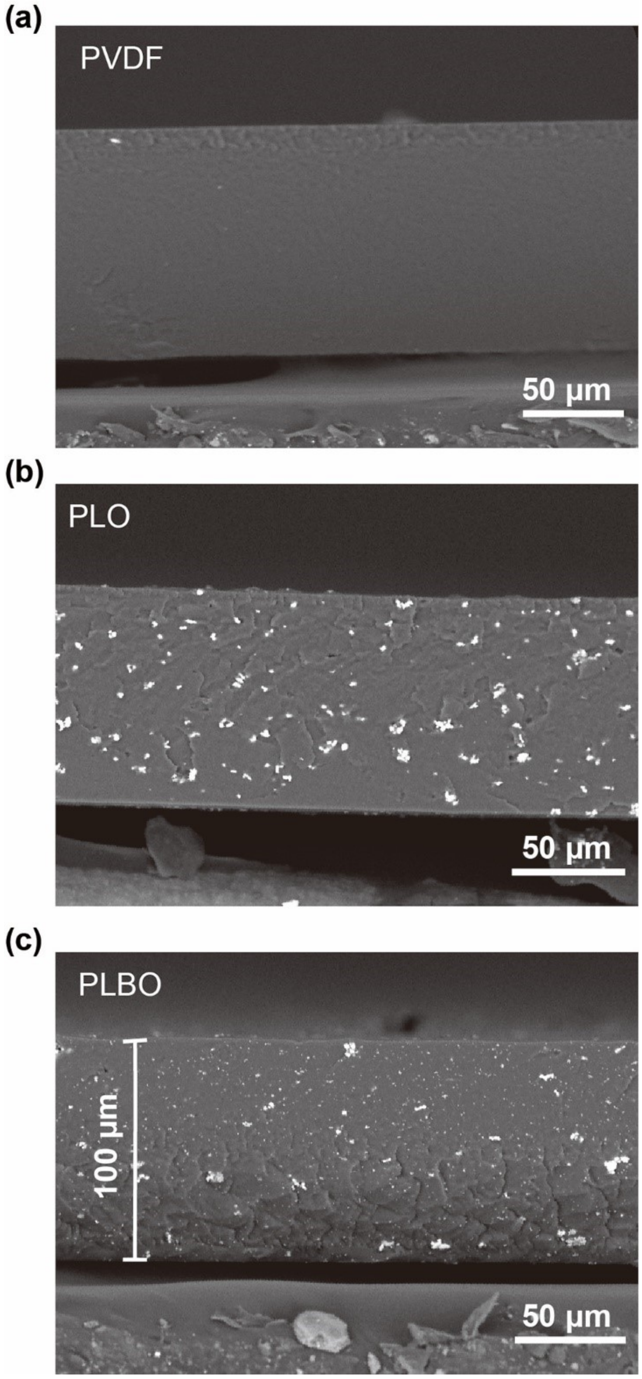

Fig. S5 cross-sectional SEM images of the (a) PVDF, (b) PLO and (c) PLBO membranes.

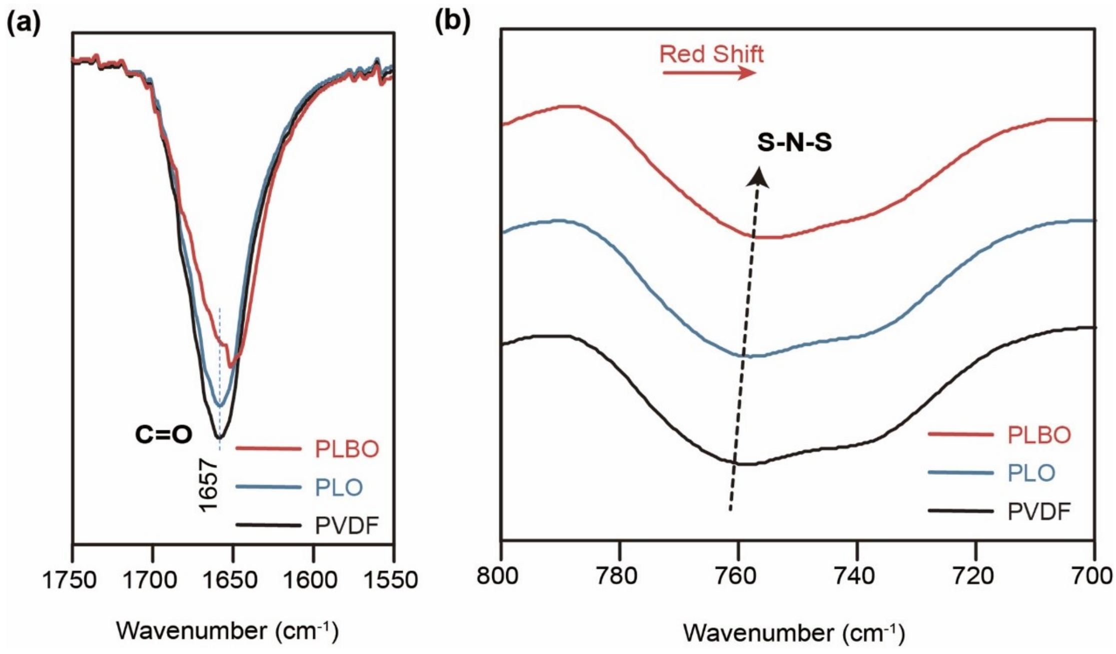

Fig. S6 FT-IR spectra of the PVDF, PLO and PLBO membranes in the range of (a) 1550-1750 cm^{-1} and (b) 700-800 cm^{-1}.

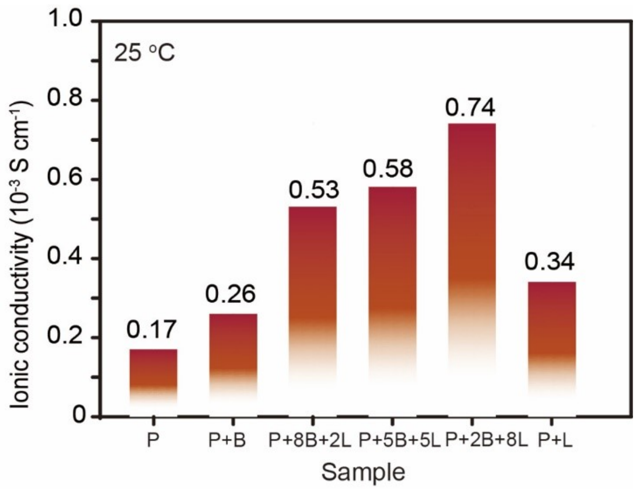

Fig. S7 Ionic conductivities of different ratio inorganic nanoparticle SPEs at 25 °C.

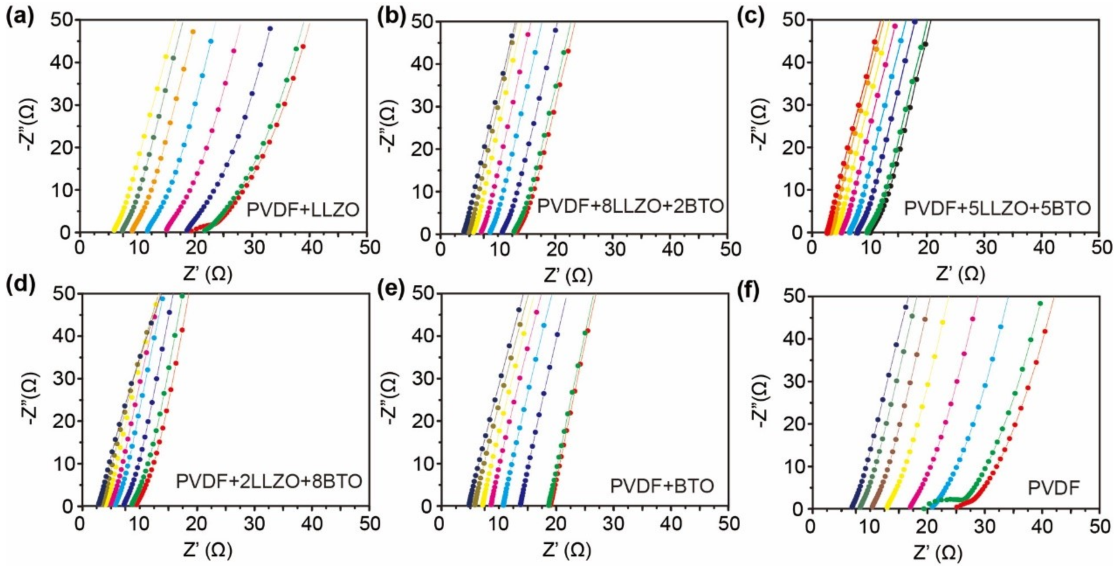

Fig. S8 EIS at different temperatures of stainless steel sheet symmetrical cells with different ratio inorganic nanoparticle SPEs

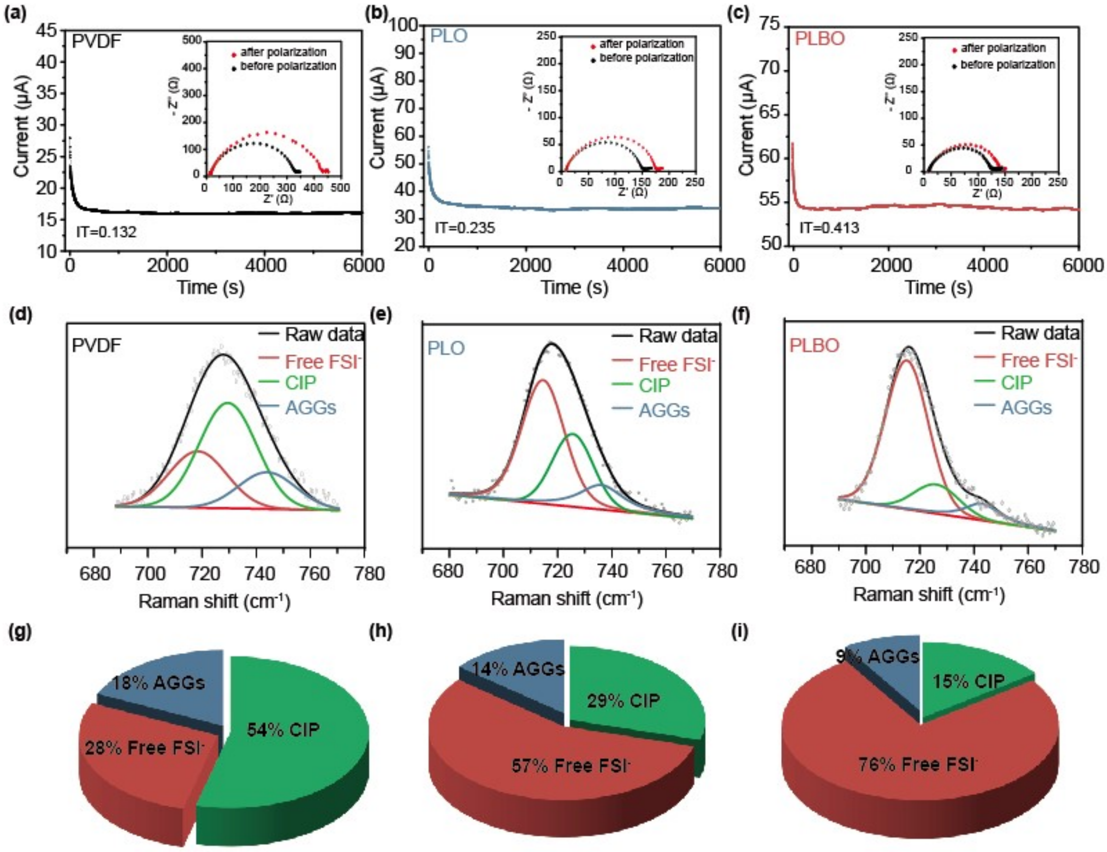

Fig. S9 The t_{Li+} of (a) Li||PVDF||Li, (b) Li||PLO||Li and (c) Li||PLBO||Li symmetrical cells and the electrochemical impedance spectroscopy (EIS) before and after dc polarization (inset). Raman spectra of the PVDF (d), PLO (e) and PLBO (f) electrolytes and corresponding quantification results of the FSI^- anion states in the electrolytes (g-i). CIP, contact ion pairs; AGGs, aggregate clusters.

Note 1: Raman spectra was exploited to examine the FSI^- anion states. From Fig. S9d-i, the content of free FSI^-, contact ion pairs and aggregate clusters in PVDF are 28%, 54% and 18%, respectively, while the corresponding values for PLBO are 76%, 15% and 9%, respectively. Introduction of BTO induces a higher concentration of free FSI^-, indicating the formation of more movable Li^+ owing to the notable dissociation of Li salt activated by BTO.

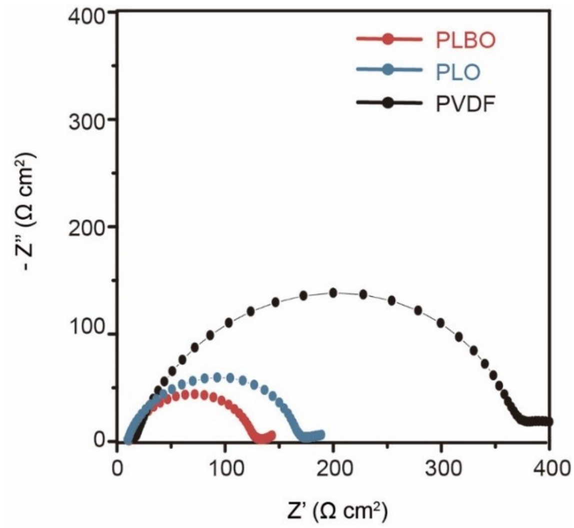

Fig. S10 EIS of Li/Li symmetric cells using PVDF, PLO and PLBO electrolytes.

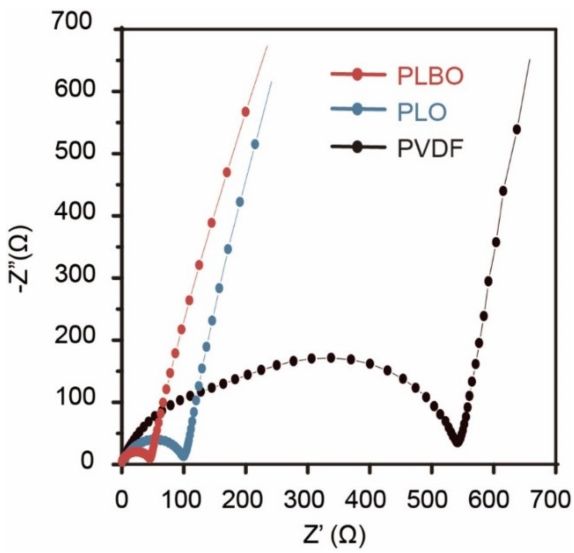

Fig. S11 EIS of solid-state NCM811||PLBO||Li, NCM811||PLO||Li and NCM811||PVDF||Li cells before cycle at 25 °C.

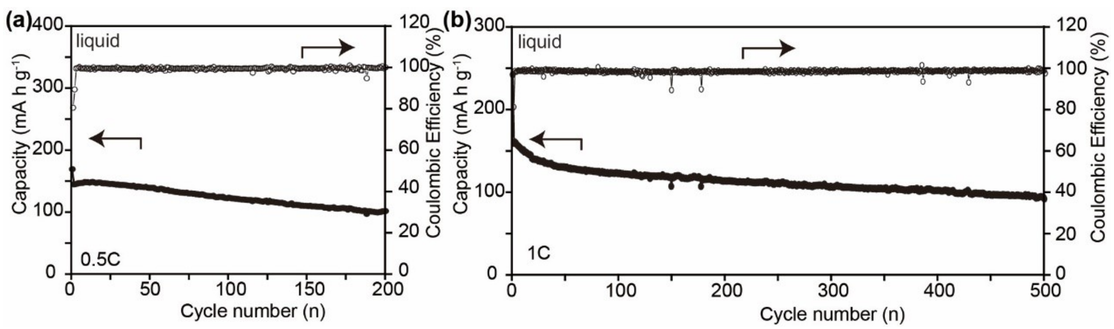

Fig. S12 Cycle performance of liquid NCM811||Li cell at (a) 0.5 C and (b) 1 C under 25 °C.

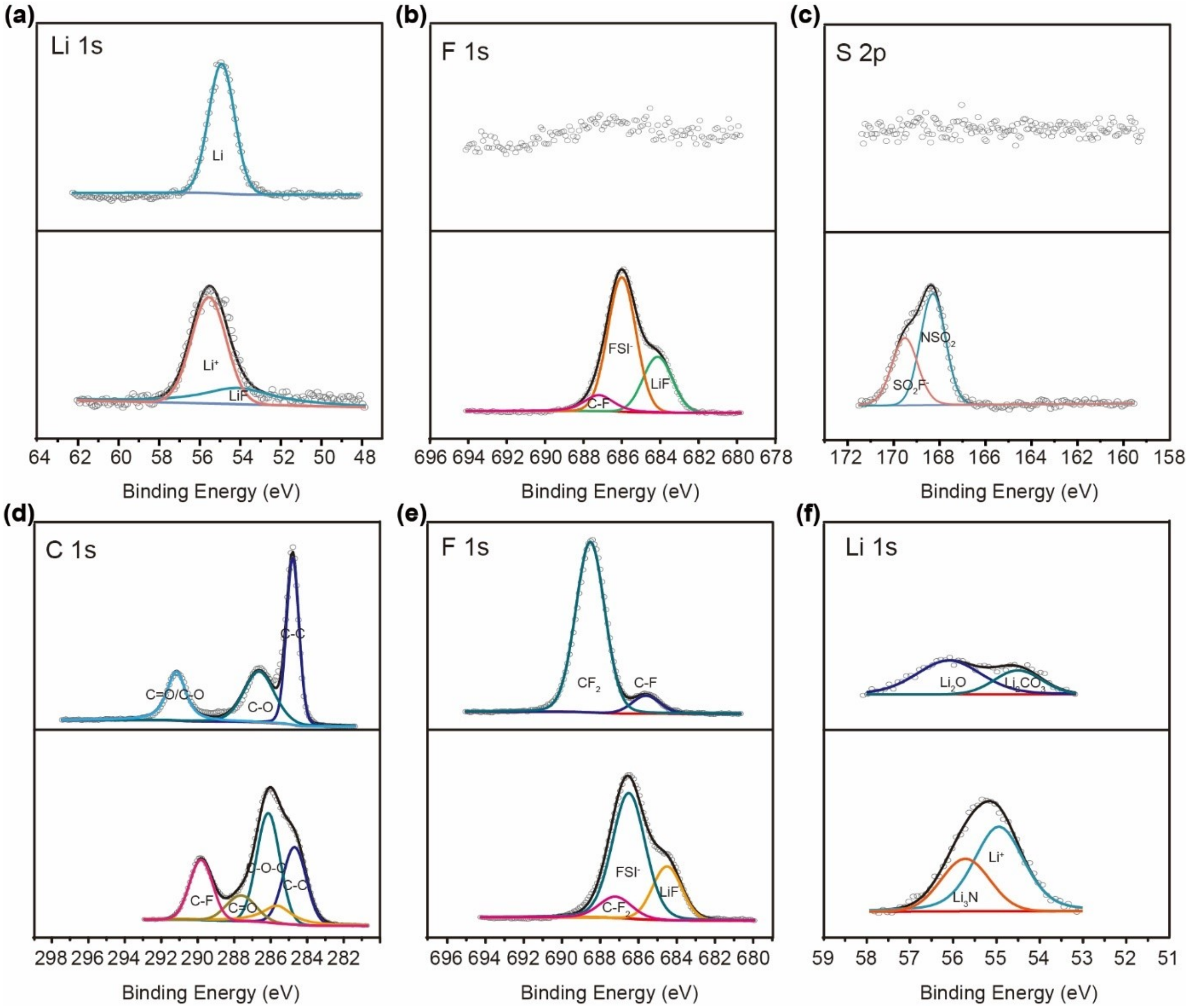

Fig. S13 XPS spectra of (a) Li 1s, (b) F 1s, and (c) S 2p of the interface layers on the Li electrodes before and after cycling. XPS spectra of (d) C 1s, (b) F 1s, and (c) Li 1s of the interface layers on the NCM 811 electrodes before and after cycling.

Note 2: The XPS analysis on the anode and cathode before and after cycling were performed to investigate the characteristics of the SEI and CEI formed on their surfaces. **Fig. S13 (a-c)** show the comparison of the lithium anode before and after cycling. According to the XPS spectra, the SEI layer formed after cycling primarily consists of LiF, Li_2CO_3, Li_2SO_x, and decomposition fragments of PVDF. New peaks for LiF appear in both the Li 1s and F 1s spectra, which is beneficial for interfacial stability and battery performance. The LiF may originate from the dehydrogenation of the PVDF chains or the decomposition of LiFSI. Species such as SO_2F^- are formed due to the decomposition of LiFSI, releasing additional F^- to form LiF. **Fig. 13 (d-f)** show the comparison of the cathode before and after cycling. According to the XPS spectra, the CEI layer formed after cycling mainly consists of LiF, Li_2CO_3, LiOH, C-F, Li_3N, and decomposition fragments of PVDF. The generated C-F peak confirms the occurrence of the dehydrofluorination phenomenon of PVDF. The production of LiF results from the reaction between lithium ions and fluorine during cycling, which helps prevent further degradation of the electrolyte. A robust CEI is conducive to the intimate coupling of solid electrolytes with electrode materials, maintaining the interfacial and structural stability of the NCM811 cathode.

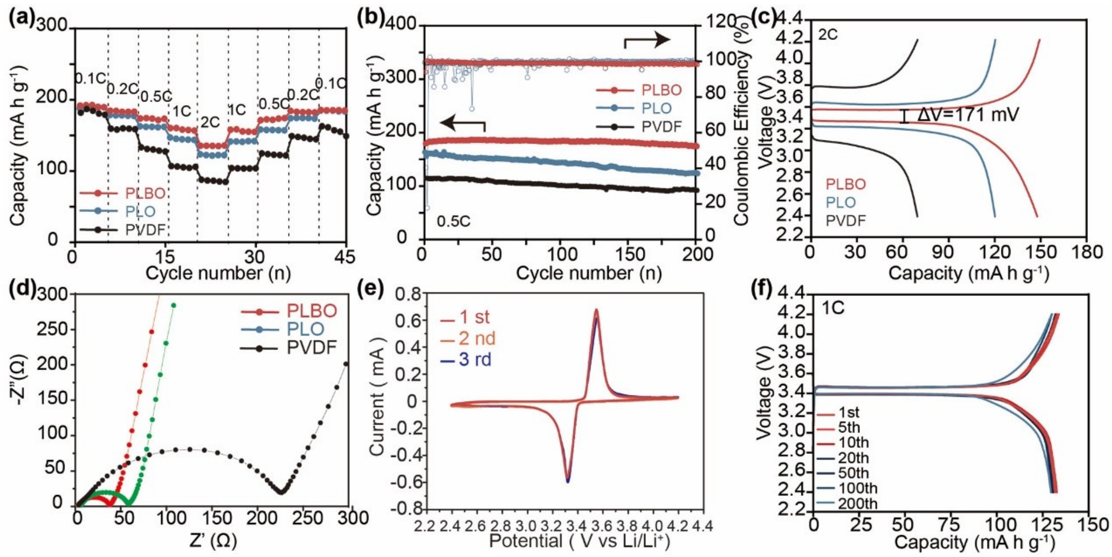

Fig. S14 (a) Rate performance of the LFP||Li solid-state batteries. (b) Cycling stability of the LFP||Li solid-state batteries at 0.5 C under 25 ℃. (c) Charge/discharge curves of LFP||Li solid-state battery at 2 C. (d) EIS of solid-state LFP||Li cells before cycle at 25 ℃. (e) CV measurements of LFP ||PLBO||Li solid-state battery at a scan rate of 0.05 mV s^{-1}. (f) Charge/discharge curves at different cycles of LFP||PLBO||Li solid-state battery.

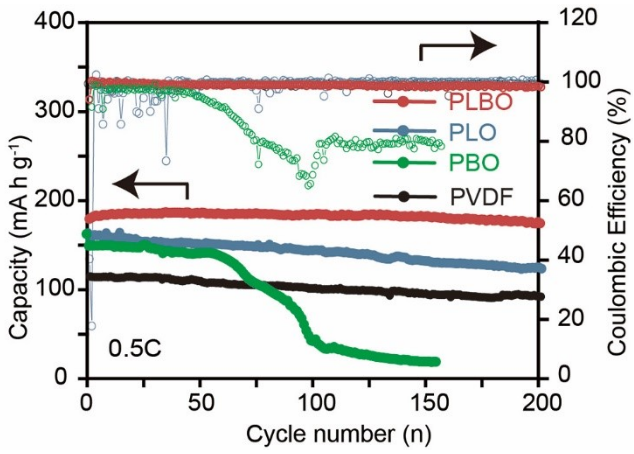

Fig. S15 Cycling stability of the LFP||Li solid-state batteries at 0.5 C under 25 ℃.

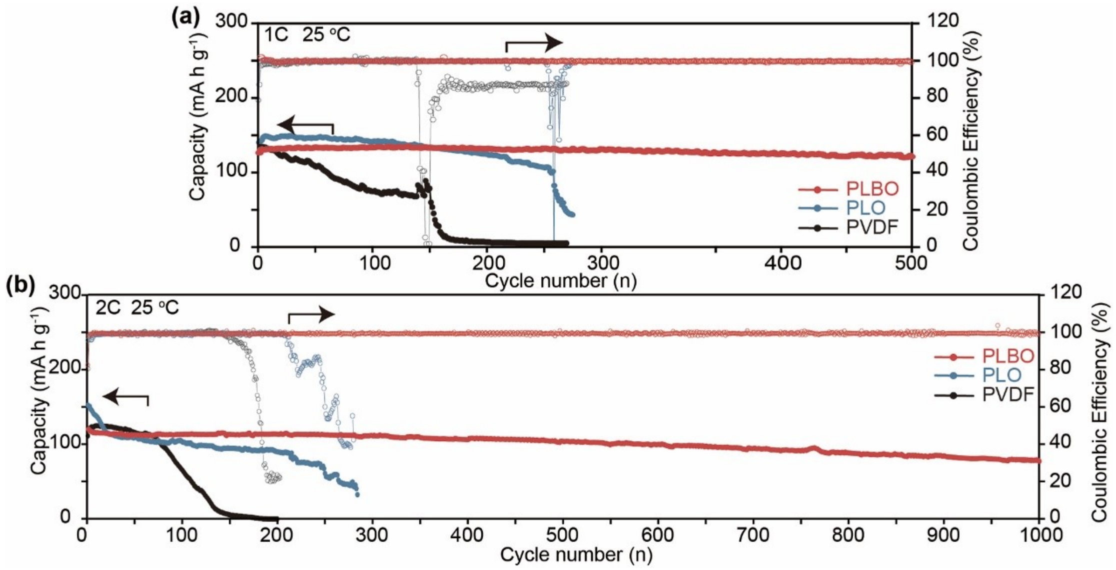

Fig. S16 Cycling stability of the LFP||Li solid-state batteries at (a) 1 C and (b) 2 C at 25 ℃.

Table S1. Performance of solid-state batteries using CSEs.

Solid state electrolyte	cell	Temperature (°C)	Rate (C)	Cycle number	Capacity after cycling (mA h g^{-1})	capacity retention (%)	Ref.
PVDF-LLZTO	$LiCoO_2$	25	0.4	120	147	98	1
PVDF-PCILs-LZSP	LFP	25	0.5	1000	140	88.5	2
	NCM811	25	0.1	200	160	81.4	
PVDF-LLTO nanofibers	LFP	25	1	100	121	99	3
PVDF-SiO_2	NCM811	25	0.5	300	173	67.5	4
PVDF-g-C_3N_4 nanosheets	NCM811	25	1	1700	112	76.6	5
PVDF-b-PTFE (PVT)- CuPcLi	LFP	25	1	1000	125	92	6
	NCM622	25	1	300	124	88	
PVDF-$Li_4Ti_5O_{12}$	LFP	35	0.5	250	150	99.7	7
PVDF- $LiTaO_3$	NCM811	25	2	740	99.3	68.3	8
PVDF-LPPO	NCM811	25	1	1550	80	70.9	9
PVDF-$NaNbO_3$	NCM811	25	2	2200	56	60	10
PVDF- $BaTiO_3$-$Li_{0.33}La_{0.56}TiO_{3-x}$	NCM811	25	1	1500	91	57.1	11
PVDF-HFP/La_2O_3	LFP	25	0.4	180	97	83	12
(PVDF)-$LiN(SO_2F)_2$	LFP	28	1	350	79.7	100	13
PVDF-LLZO-$BaTiO_3$ (noted as PLBO)	**LFP**	**25**	**1**	**500**	**119.5**	**92**	**Our work**
			2	**1000**	**80.1**	**70**	
	NCM811	**25**	**0.5**	**200**	**101**	**80.7**	
			2	**700**	**73**	**81**	

References

1 X. Zhang, T. Liu, S. Zhang, X. Huang, B. Xu, Y. Lin, B. Xu, L. Li, C.-W. Nan and Y. Shen, Synergistic Coupling between $Li_{6.75}La_3Zr_{1.75}Ta_{0.25}O_{12}$ and Poly(vinylidene fluoride) Induces High Ionic Conductivity, Mechanical Strength, and Thermal Stability of Solid Composite Electrolytes, *J. Am. Chem. Soc.*, 2017, **139**, 13779-13785.

2 L. Zhu, J. Chen, Y. Wang, W. Feng, Y. Zhu, S. F. H. Lambregts, Y. Wu, C. Yang, E. R. H. van Eck, L. Peng, A. P. M. Kentgens, W. Tang and Y. Xia, Tunneling Interpenetrative Lithium Ion Conduction Channels in Polymer-in-Ceramic Composite Solid Electrolytes, *J. Am. Chem. Soc.*, 2024, **146**, 6591-6603.

3 B. Li, Q. Su, L. Yu, D. Wang, S. Ding, M. Zhang, G. Du and B. Xu, $Li_{0.35}La_{0.55}TiO_3$ Nanofibers Enhanced Poly(vinylidene fluoride)-Based Composite Polymer Electrolytes for All-Solid-State Batteries, *ACS Appl. Mater. Interfaces*, 2019, **11**, 42206-42213.

4 Y. Ma, C. Wang, K. Yang, B. Li, Y. Li, S. Guo, J. Lv, X. An, M. Liu, Y.-B. He and F. Kang, Ultrathin and Robust Composite Electrolyte for Stable Solid-State Lithium Metal Batteries, *ACS Appl. Mater. Interfaces*, 2023, **15**, 17978-17985.

5 L. Chen, T. Gu, J. Ma, K. Yang, P. Shi, J. Biao, J. Mi, M. Liu, W. Lv and Y.-B. He, In situ construction of Li_3N-enriched interface enabling ultra-stable solid-state $LiNi_{0.8}Co_{0.1}Mn_{0.1}O_2$/lithium metal batteries, *Nano Energy*, 2022, **100**, 107470.

6 H. Wang, H. Cheng, D. Li, F. Li, Y. Wei, K. Huang, B. Jiang, H. Xu and Y. Huang, Lithiated Copper Polyphthalocyanine with Extended π‐Conjugation Induces LiF‐Rich Solid Electrolyte Interphase toward Long‐Life Solid‐State Lithium‐Metal Batteries, *Adv. Energy Mater*, 2023, **13**, 2204425.

7 Q. Zhou, X. Yang, X. Xiong, Q. Zhang, B. Peng, Y. Chen, Z. Wang, L. Fu and Y. Wu, A Solid Electrolyte Based on Electrochemical Active $Li_4Ti_5O_{12}$ with PVDF for Solid State Lithium Metal Battery, *Adv. Energy Mater*, 2022, **12**, 2201991.

8 Y. Yuan, L. Chen, Y. Li, X. An, J. Lv, S. Guo, X. Cheng, Y. Zhao, M. Liu, Y.-B. He and F. Kang, Functional $LiTaO_3$ filler with tandem conductivity and ferroelectricity for PVDF-based composite solid-state electrolyte, *Energy Materials and Devices*, 2023, **1**, 9370004.

9 J. Mi, J. Ma, L. Chen, C. Lai, K. Yang, J. Biao, H. Xia, X. Song, W. Lv, G. Zhong and Y.-B. He, Topology crafting of polyvinylidene difluoride electrolyte creates ultra-long cycling high-voltage lithium metal solid-state batteries, *Energy Storage Mater*, 2022, **48**, 375-383.

10 X. An, Y. Liu, K. Yang, J. Mi, J. Ma, D. Zhang, L. Chen, X. Liu, S. Guo, Y. Li, Y. Ma, M. Liu, Y. B. He and F. Kang, Dielectric Filler‐Induced Hybrid Interphase Enabling Robust Solid‐State Li Metal Batteries at High Areal Capacity, *Adv. Mater.*, 2023, **36**, 2311195.

11 P. Shi, J. Ma, M. Liu, S. Guo, Y. Huang, S. Wang, L. Zhang, L. Chen, K. Yang, X. Liu, Y. Li, X. An, D. Zhang, X. Cheng, Q. Li, W. Lv, G. Zhong, Y.-B. He and F. Kang, A dielectric electrolyte composite with high lithium-ion conductivity for high-voltage solid-state lithium metal batteries, *Nat. Nanotechnol.*, 2023, **18**, 602-610.

12 Y. Zeng, L. Zhao, J. Zhang, Q. Li, D. Sun, Y. Ren, Y. Tang, G. Jin and H. Wang, La_2O_3 Filler's Stabilization of Residual Solvent in Polymer Electrolyte for Advanced Solid‐State Lithium‐Metal Batteries, *Small Science*, 2023, **3**, 2300017.

13 Q. Kang, Y. Li, Z. Zhuang, D. Wang, C. Zhi, P. Jiang and X. Huang, Dielectric polymer based electrolytes for high-performance all-solid-state lithium metal batteries, *J. Energy Chem*, 2022, **69**, 194-204.